Available online at www.sciencedirect.com
SCIENCE DIRECT
Thin Solid Films 500 (2006) 330 – 335
thin solid films
www.elsevier.com/locate/tsf

Temperature stability of thin anodic oxide films in metal/insulator/metal structures: A comparison between tantalum and aluminium oxide

Yanka Jeliazova [a], Michael Kayser [a], Beate Mildner [a], Achim Walter Hassel [b], Detlef Diesing [a,*]

[a] Fachbereich Chemie, Universität Duisburg-Essen, 45117 Essen, Germany
[b] Max-Planck-Institut für Eisenforschung, Max-Planck-Str. 1, 40237 Düsseldorf, Germany

Received 5 April 2005; received in revised form 18 October 2005; accepted 31 October 2005
Available online 4 January 2006

Abstract

The dielectric breakdown of thin ($d=3-4$ nm) aluminium and tantalum oxide films was investigated by means of current voltage plots in metal/insulator/metal systems. Dielectric breakdown field strengths, E_{DB}, of 0.6 GV m^{-1} were found for both oxide types at room temperature. Differences appear in the temperature dependence of E_{DB}. Tantalum oxide films show an unchanged breakdown behaviour for temperatures up to 420 K while aluminium oxide films lose already 80% of their E_{DB} value in the same temperature range. Time-resolved investigations of the electric breakdown revealed intermediate states of both oxide types which were stable for several ms being characterized by an enhanced tunnel current. The breakdown voltage clearly scales with the oxide thickness for both oxide types.
© 2005 Elsevier B.V. All rights reserved.

Keywords: Tantalum oxide; Aluminum oxide; Dielectric properties; Tunnelling

1. Introduction

Dielectric breakdown (further called DB) of thin oxide films may be caused by a number of alternative processes. These are, for instance, field-induced ionization, doping, crystallisation, breaking of chemical bonds, and migration of lattice defects. Sample properties such as conductivity, temperature or stress will run away uncontrollably when these processes set in with a positive feedback without equilibrating factor. The stored field energy $1/2\cdot\epsilon_0\cdot\epsilon_r\cdot E^2$ (ϵ_r: relative permittivity, ϵ_0: vacuum polarization) is then released in a may be very narrow region, for example a single conduction path induced by defect ions or voids. This may cause mechanic defects of the samples. Eventually, they lose their original properties as rectifiers or capacitors.

A large body of literature exists concerning investigations of dielectric breakdown. Some earlier works lead to an overview over this wide field [1–6]. Within the last years, several new reports were published elucidating the breakdown phenomenon experimentally [7,8] and by theoretical approaches, see for example Refs. [9,10]. The theoretical works focused mainly on field-induced growth phenomena of conducting paths through oxide films. Treelike damage structures in the insulator were observed. Their exact shape and fractal structure were calculated and found to depend on the temperature [11]. However, there is a lack in experimental literature concerning the temperature dependence of DB. In complementary metal oxide semiconductor (CMOS) circuits, thin oxide layers have to withstand high field strengths (0.1–1 GV m^{-1}) even at elevated temperatures. For this reason, the present work wants to deliver data and a microscopic insight in DB phenomena for temperatures 300 K$<T<$500 K.

We have chosen alumina ($\epsilon_r\approx 12$) and tantalum oxide thin films ($\epsilon_r\approx 28$) for our investigations since they are currently considered as suitable materials for miniaturized metal oxide semiconductor field effect transistors [12] and capacitors [13–17]. Capacitors ($C=\epsilon_0\cdot\epsilon_r\cdot A/d$) in integrated circuits, for instance, are preferred to have a thin insulator layer, d, rather than a large electrode area, A, to provide high values of C and a small device size simultaneously.

DB phenomena in thin films ($d<4$ nm) might differ from the ones observed in thick dielectrics ($d>10$ nm). In the former case, a considerable contribution to the breakdown current is due to the tunnel effect which is often neglected in literature

* Corresponding author.
E-mail address: detlef.diesing@uni-due.de (D. Diesing).

0040-6090/$ - see front matter © 2005 Elsevier B.V. All rights reserved.
doi:10.1016/j.tsf.2005.10.088

[18]. Thereby a part of the theoretical models based on ionization and ionic transport currents cannot be applied for DB in thin films. In the present work, DB currents will consequently be discussed in terms of tunnel currents through modified tunnel barriers. A small theoretical treatise on the calculation of absolute tunnel current densities is therefore added in the Discussion.

2. Experimental details

2.1. Electrochemistry

The substrates for the preparation of the metal/metal oxide/metal tunnel junctions were flat plates of SiO_2. The aluminium films (d=20 nm) were thermally evaporated in a high vacuum chamber at a pressure of 10^{-6} Pa. The tantalum films (d=20 nm) were evaporated by means of an e-beam. The details and the geometry of the samples are given elsewhere [19].

The localized anodic oxidation was performed in a droplet cell, see Fig. 1.

The thickness of the anodic oxide film can be adjusted by a cyclic voltammogram from 1.2 nm to 10 nm with a precision of 0.1 nm [19]. The thickness control is done by the method of further anodic oxide growth and ellipsometric measurements [20]. Sample and sample holder with the oxidized Al/Ta films and the necessary electrical connections were then transferred into the UHV system with a base pressure of $4 \cdot 10^{-8}$ Pa, where the top metal film (gold) was evaporated onto the metal/metal oxide system with a thickness of 15 nm. The contact area of the junction was 2 mm·4 mm. In the UHV apparatus the sample was mounted on a copper holder with a thermoelement attached on the back side. The electronic equipment consisted of a fast rising potentiostat (rise time<300 ns) and a pulse generator system (-10 V$<U_{pulse}<$10 V).

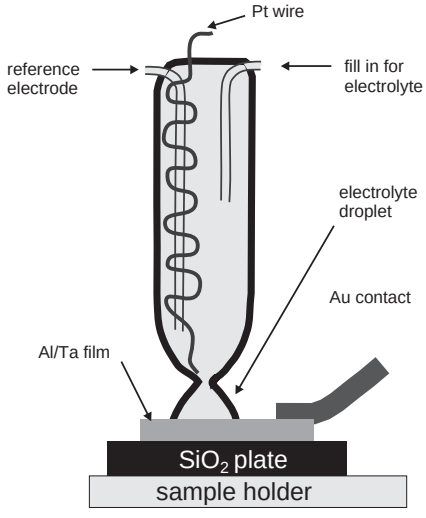

Fig. 1. Anodic oxidation of Al and Ta thin films in a droplet cell. In one quartz tube the electrolyte can be filled, the other tube contains the salt bridge to the reference electrode. The platinum wire acts as counter electrode. The Al/Ta film itself is the working electrode, which is contacted by a gold wire in the part of the film, which is not oxidized.

3. Results

3.1. Dielectric breakdown processes in the time domain

In the first experiment, the DB event was studied by monitoring the tunnel current after switching on a voltage which induces the dielectric breakdown. The electrochemically produced oxide layers used in this work are known to have a sharply defined breakdown field strength of 0.55 GV m^{-1} and 0.64 GV m^{-1} for tantalum oxide and alumina [21], respectively. Consequently, the breakdown voltages for the 3.2-nm-thick oxide layers are U_{DB}(Al)=2.11 V and U_{DB}(Ta)=1.76 V. In the experiment the applied voltages were chosen 10% higher than the U_{DB} values (2.3 V for Al and 2.0 V for Ta).

Fig. 2 shows typical transients for both oxide systems after the application of the breakdown voltage with a logarithmic time and current scale. Both tunnel systems suffered a dielectric breakdown. The current exceeded values of 0.1 A and the samples lost their capacitance after switching off the voltage. However, the characteristics of the current transients are quite different for the two systems.

For Ta samples, the current is constant for a quite long time of t=12 ms. Then the current suddenly increases by a factor of 2.5. This value remains again constant up to t=0.2 s, then the current increases for a second time (factor of 3.6). The second event lasts 170 ms. Subsequently, the sample current increases up to values of 0.1 A and the capacitance of the sample is irreversibly lost. The step like increase of the tunnel current before the DB could be observed for all of our samples. These events seem to proceed always as a kind of precursor of the dielectric breakdown.

The AlOx samples show a much lower tunnel current (≈3 magnitudes), albeit the oxide thickness is equal and the applied tunnel voltage is even 0.3 V higher. This difference is caused by the fact that electrochemically prepared alumina films have quite high tunnel barriers (2.4 eV–4 eV) [22]. Tantalum oxide mediated tunnel barriers are much lower (1.7 eV, see Fig. 5) and the devices show therefore a higher tunnel probability. The transient of the DB current shows sudden increases similar to the TaOx samples, but the time needed for the first current increase is smaller (1.5 ms) and the subsequent current increases also occur after much shorter delays. The final breakdown event is finished after 2.4 ms.

An interesting question is whether these precursor events lead already to a partial destruction of the sample. In a previous work, a current comparator was used to trap the MIM (metal/insulator/metal) junction after a current increase before the DB. The current comparator switched the voltage off when the current increased from its initial value by a factor of 2 [18]. The experiment was then restarted and it was found that the samples capacitance was not changed, but its conductivity was reduced. Subsequently, the breakdown voltage was increased and the samples were stable for voltages higher than U_{DB}.

The same behaviour was observed in the present experiment for the Al and Ta samples. Higher voltages than U_{DB} could be applied in fast voltage sweeps (dU/dt=10 V s^{-1}) without breakdown. Such a treatment also leads to a significant reduction of conductivity with an unchanged capacitance.

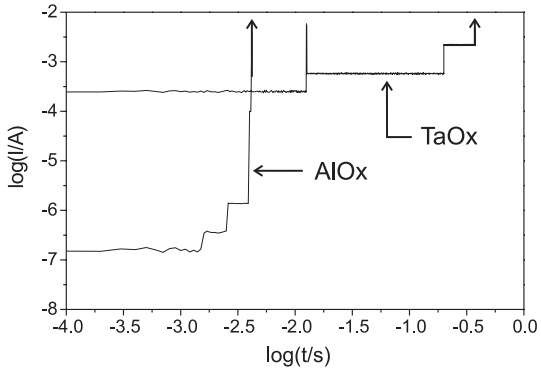

Fig. 2. Current transient of Al/AlOx/Au and Ta/TaOx/Au tunnel junctions with 3.2 nm thick insulator layers after switching the voltage from 0 V to U_{DB} (U_{DB}(Al)=2.3 V, U_{DB}(Ta)=2.0 V). Breakdown events indicated by upwards directed vertical arrows.

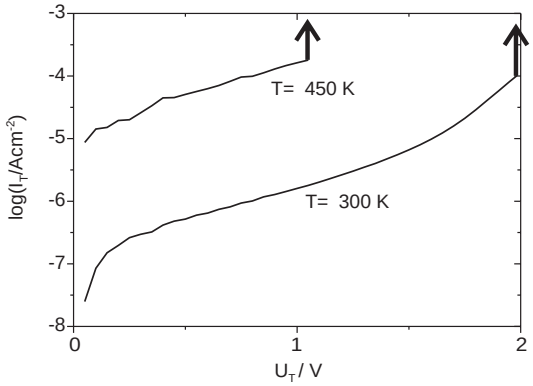

Fig. 4. Current voltage plot of a Ta/TaOx/Au tunnel junctions at temperatures T=300 K and T=450 K with d_{oxide}=3.2 nm. Breakdown events indicated by upward arrows.

Therefore, the observed precursor events occurring before the DB cannot be assigned to a growth of conductive channels through the oxide. These channels should remain in the oxide when the experiment is restarted and the samples conductivity should be increased. In the potentiostatic experiment, however, the precursor events of the DB always increase the sample conductivity and the precursors finally lead to the DB when the voltage is not switched off.

A reason for the observed current increases may be the existence of mobile charge carriers (e.g. Al^{3+} and O^{2-}) in the oxide. Mobile ions are necessary for the electrochemical oxidation, which is a consumptive method. The oxide growth takes place on the metal/oxide interface as well as on the oxide/electrolyte interface by simultaneous migration of cations and anions through the oxide. When the oxidation cyclovoltammogram is finished, excess ions remain in the oxide lattice. These ions may move in an electric field due to thermal activation. Consequently, we investigated the DB phenomenon as a function of sample temperature.

3.2. Dielectric breakdown processes as function of temperature

In Fig. 3, the current–voltage plots (dU/dt=2 mV s^{-1}) of an Al/AlOx/Au tunnel junction is shown at temperatures 300 K and 360 K. The observed currents are below the signal/noise ratio for voltages up to 1 V. Then an exponential current increase sets in and the sample breaks down at 300 K with a tunnel voltage U_T=2 V. At T=360 K the current observed for tunnel voltages U_T<1.4 V is not significantly increased but the samples suffer the DB already at 1.4 V. The moderate current increase from 300 K to 360 K is a typical property for Al/AlOx tunnel junctions since their high tunnel barriers suppress an increase of the tunnel current due to thermally excited electrons.

In contrast to this, the TaOx samples show a significant temperature dependence of the tunnel current. An increase by a factor of 4 for the tunnel current at U_T=1 V was observed when the sample was heated from 300 K to 360 K. However, no significant change of the DB voltage (U_{DB}=2 V) at 300 K was found when the sample was annealed to 360 K. Further annealing to 450 K leads to a decrease of the DB voltage to 1 V (see Fig. 4). The current up to 1 V is increased by nearly two orders of magnitude. The reason for this can be seen in the low barrier heights for TaOx tunnel junctions. A calculation of the temperature dependence is given in the Discussion.

Barrier heights in tunnel junctions can be determined by the onset of Fowler–Nordheim tunnelling [22,23]. In this case, the energy of the tunnelling electrons $e \cdot U_T$ overcomes the height

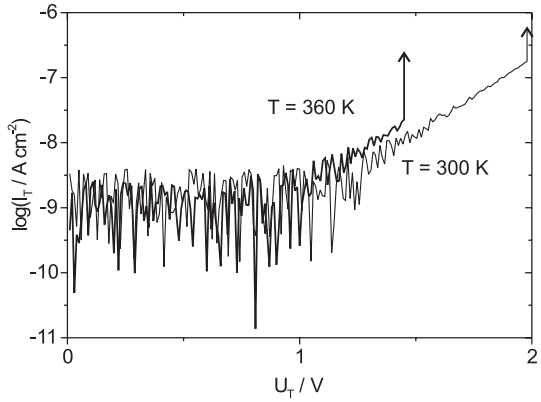

Fig. 3. Current voltage plot of Al/AlOx/Au tunnel junctions at temperatures T=300 K and T=360 K with d_{oxide}=3.2 nm. Breakdown events indicated by upward arrows.

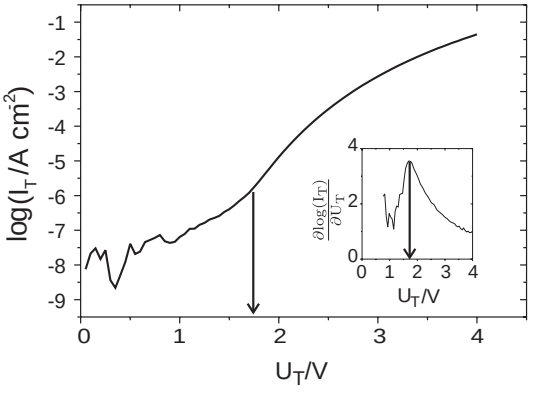

Fig. 5. Current voltage plot of a Ta/TaOx/Au tunnel junction with d_{oxide}=3.6 nm taken at T=92 K. Inset: Logarithmic derivative. Both plots show the onset of Fowler–Nordheim tunnelling at U_T=1.7 V.

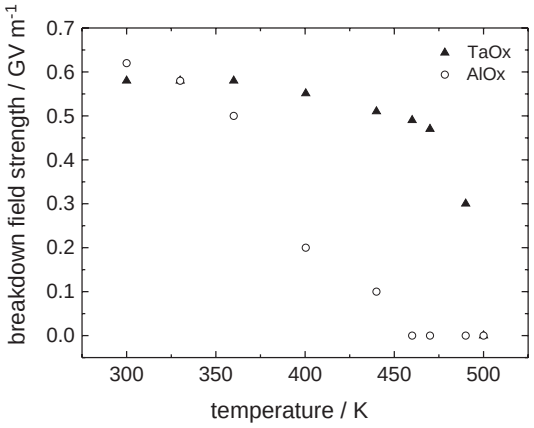

Fig. 6. Evaluation of the breakdown voltage as function of the sample temperature.

of the tunnel barrier $e \cdot \varphi$ leading to a characteristic slope change in the logarithmic current voltage plot. In Fig. 5 a plot is shown for a TaOx tunnel junction with an inset showing the logarithmic derivative as a function of the tunnel voltage. A maximum of the derivative and a slope change in the current plot can be found at $U_T = 1.7$ V indicating a barrier height of 1.7 eV for TaOx tunnel junctions.

A collection of measured breakdown voltages for oxide layers with the mentioned thickness of 3.2 nm is given in Fig. 6. The AlOx tunnel junctions lose 50% of their DB field strength already at 400 K while the TaOx samples show an unchanged stability at this temperature. A decrease for these samples sets in at $T > 450$ *K* and at $T > 500$ K the samples show an immediate DB. For AlOx samples the immediate DB appears already at 450 K. The TaOx samples seem to withstand temperatures up to 500 K without any damage. After the samples were cooled down, they show the same behaviour as observed before the heating. The resistance of the tantalum and gold films was measured separately and found to be also unchanged.

4. Discussion

4.1. Temperature dependence of tunnel currents

A surprising result of the experiments presented here is the fact that TaOx tunnel junctions show an unchanged DB behaviour from 300 K to 450 K, whereas a significant temperature dependence was found for the tunnel current. In the literature, the temperature dependence of currents in oxide devices is often discussed in terms of ionic conduction [20,24]. This is not appropriate for the present work. In thin film tunnel junctions an ionic current would diminish the thickness of the two metal electrodes and cause a resistivity change. Since this is not observed even when the measurements are performed for hours at elevated temperatures, this ionic transport should be excluded and one has to work out the details about the temperature dependence of electronic tunnelling.

As a starting point, let us consider the magnitude of the incoming electron flux j (electrons $m^{-2}\ s^{-1}$) at the metal/oxide interface. If the number of electrons which are attempting to tunnel is known, one can multiply the incoming particle flux with the tunnel probability yielding the transmitted current through the oxide (tunnel current) in A m^{-2}. The incident current density for example at the Al/oxide interface may be represented as $j_\perp = n \cdot e \cdot v_\perp$, where n is the electron density and $v_\perp$ denotes the velocity component of the electron perpendicular to the interface. It can be given as $\frac{1}{\hbar}\frac{\partial E}{\partial k_\perp}$ ($k_\perp$ being the wave vector component normal to the metal/oxide interface). We can express the electron density n as $\int f(E,T)\frac{d^3k}{(2\pi)^3} = \frac{N}{V}$ where $f(E,T)$ is the Fermi function at the temperature T.

The flux $j_\perp$ then becomes

$$j_\perp = 2e\int f(E,T)v_\perp \frac{d^3k}{(2\pi)^3} \tag{1}$$

We proofed the numerical calculations by setting e and $v_\perp$ to unity in Eq. (1). Then, considering the value of $E_F = 11.7$ *eV* for the Al base electrode [25] the right hand side of the equation gives the value of $1.81 \cdot 10^{29}$ m^{-3} for the electron density [26]. Using a free electron dispersion $E = \frac{\hbar^2}{2m}\left(k_{||}^2 + k_\perp^2\right)$ ($k_{||}$ is the wave vector component parallel to the metal/oxide interface), the k integration can be splitted in one for the normal and one for the parallel component. This is desirable since only electrons with positive $k_\perp$ will attempt the tunnel process. The electron flux at the interface can then be expressed as:

$$j_\perp = 2e\int_{-\infty}^{+\infty}\frac{d^2k_{||}}{(2\pi)^2}\int_0^{+\infty}\frac{dk_\perp}{(2\pi)}f(E)\frac{\hbar k_\perp}{m} \tag{2}$$

When two metal films under a bias voltage U_T are brought into contact, the term $f(E)$ in Eq. (2) has to be replaced by

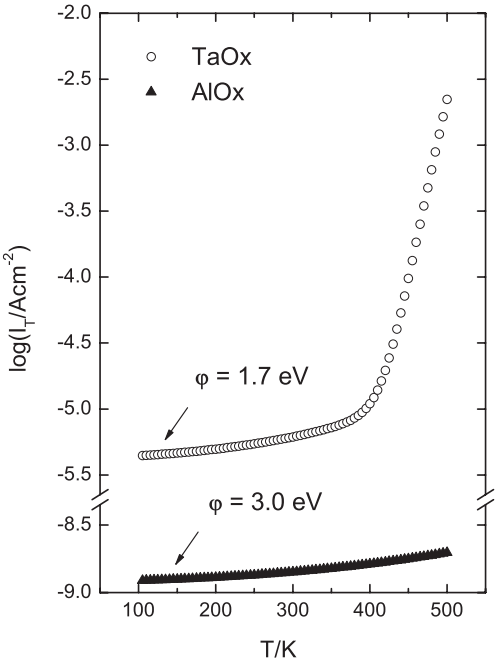

Fig. 7. Calculation of the tunnel current density at $U_T = 1$ V through a 3.2-nm-thick oxide barrier with different barrier heights ($\phi = 1.7$ eV for Ta and $\phi = 3.0$ eV for Al). The tunnel current is plotted in logarithmic scale as function of the sample temperature.

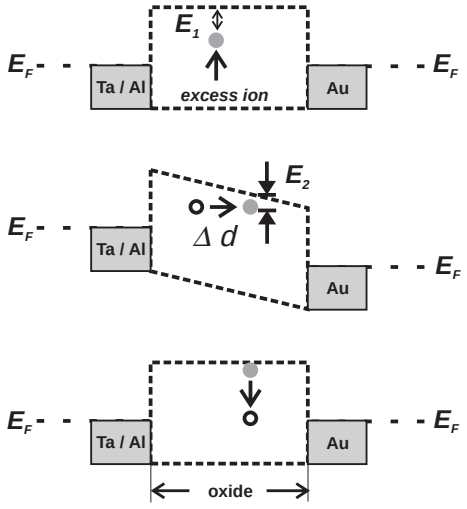

Fig. 8. A model of a tunnel junction with an excess ion in the barrier. Upper viewgraph: $U_T=0$ V. The ions energy with respect to the conduction band minimum E_{CB} is E_1. Middle viewgraph: Applied tunnel voltage leads to a hopping of the ion and an energy gain $\Delta E=E_2-E_1$ with respect to E_{CB}. Bottom viewgraph: Relaxation of the ion after the tunnel voltage is switched off.

$f(E)\cdot(1-f(E+e\cdot U_T))$ [27]. As a whole, this means that only occupied electronic states with non-vanishing positive momentum component normal to the oxide interface will try to tunnel into free electronic states of the opposing metal film. For a bias voltage of $U_T=1$ V one calculates with Eq. (2), for example, a flux of $1\cdot10^{34}$ electrons m^{-2} s^{-1} which probe the tunnel process at the aluminium/oxide interface. The product of the incoming electron flux and the tunnel probability leads to the tunnel current density. The tunnel probability can be obtained using the semiclassical WKB (Wentzel–Kramers–Brillouin) approximation [28] and has to be included in Eq. (2) (for details see Wolf [27]).

In Fig. 7, the temperature dependence of the calculated elastic electron tunnel current at $U_T=1$ V is shown. The current is plotted logarithmically for barrier heights of 1.7 eV and 3.0 eV. The tunnel current through the 3.0 eV high barrier varies over the temperature range from 300 K to 450 K only by several percentages, while it increases by 1.5 orders of magnitude for 1.7 eV high barrier. For such low barriers, a Fowler–Nordheim tunnel process is allowed for a part of the thermally excited electrons at 450 K at tunnel voltages $e\cdot U_T<\phi$. This is not the case for the higher barriers and the temperature dependence is much weaker. The experimentally observed increase for TaOx was 2 orders of magnitude. This difference may only partially be due to thermally activated electron hopping conduction through the oxide. The dominating effect leading to the pronounced temperature dependence of the tunnel currents in TaOx samples can be explained in terms of elastic electronic tunnelling through a 1.7 eV high barrier. This agrees well with the barrier height, which was determined experimentally by the onset of Fowler–Nordheim tunnelling in Fig. 5. The experimentally observed weak temperature dependence of AlOx samples is reasonable since the calculation also predicts a weak dependence for barrier heights of 3.0 eV (Fig. 7).

4.2. Tunnel current changes before dielectric breakdown

It was already mentioned that the experimentally observed tunnel current changes before DB displayed in Figs. 3 and 4 cannot be explained by a growth of conductive channels through the oxide. Different DB procedures have to be found. The electrochemically prepared oxide films are amorphous, they are often called vitreous films [29]. Defect ions in connected potential wells (so-called tunnelling states) are responsible, for example, for the high heat capacity of vitreous oxides [29] and for dielectric relaxation phenomena [30].

Electrochemical oxide films contain excess cations and anions due to the growth mechanism, which is based on the hopping of ions through the oxide film. The field induced hopping may start again when the bias voltage is applied to the MIM junction. Due to the applied voltage, the mobile species may gain energy with respect to the oxides conduction band $\Delta E=(E_2-E_1)$ during a hop of distance Δd (Fig. 8).

The excess ion is then near to the conduction bands minimum which changes the band structure of the oxide slightly influencing also the tunnel barrier in the junction. Using Eq. (2) one can estimate the barrier changes which are necessary to explain the current increase before DB in Figs. 4 and 3. When a 3.0-eV-high barrier is reduced by 0.1 eV, the tunnel current will increase by a factor of ≈ 3, while a factor of ≈ 6 is calculated for a 1.7 eV barrier.

Obviously, changes of 0.1 eV in the barrier height are sufficient to explain the current increases which are observed before DB. However, it is not possible with the present data to assign the observed phenomena to a real band structure change in the oxide. The excess ion may serve after the hop also as a centre for resonance tunnelling, which would also explain the tunnel current increase. Since the current increases stepwise (Fig. 2) with a length of the steps of several ms, it is possible to assign this step length to a metastable state with a lifetime τ.

The attempt frequency ν for hopping events can be taken from the phonon frequency in the oxide [31] (mean value $\nu=10^{14}$ s^{-1} [32]). The necessary waiting time for a hopping event with an activation energy E_{act} can then be written as

$$\tau=\frac{1}{\nu}e^{\frac{E_{act}}{k_bT}} \tag{3}$$

where k_b is the Boltzmann constant and T is the sample temperature [33]. For the experiment with the tantalum tunnel systems, the duration between two tunnel current changes up to 100 ms. Using Eq. (3) this time would correspond to an activation energy of 0.77 eV at room temperature. One has to take into account that at an applied tunnel voltage of 2 V the voltage drop across the whole oxide film (≈ 12 atomic layers) corresponds to a potential difference of 0.16 eV between each atomic layer. Thereby a hop of an ion starting in an interstitial position along a path of two or three atomic layers can motivate the fact that ions in TaOx can defray this estimated activation energy.

For the AlOx samples the lifetime of the metastable state was shorter (≈ 1 ms). This would correspond to an activation energy of 0.65 eV which is by 0.1 eV lower than for TaOx. A

lower activation energy for ion hops would also explain the pronounced temperature dependence of the DB for the AlOx samples. With the present data set an exact model for the temperature dependence of the DB could not be developed. Additional experiments studying the metastable state lifetime as a function of the temperature would be necessary. Then we expect that the temperature dependence of the activation energy will allow to derive a detailed picture of the kinetics in dielectric breakdown.

5. Conclusion

Amorphous TaOx films were found to be stable in metal/insulator/metal devices up to temperatures of 500 K. The breakdown stability was found to be nearly constant at 300 $K < T < 450$ K. Metastable states of increased tunnel currents appear always as precursors of the breakdown. They can be explained as tunnel currents through slightly reduced tunnel barriers. The AlOx films were found to be less stable at elevated temperatures. The different behaviour can be rationalized by different activation energies for ionic hopping in the oxide.

Acknowledgements

The authors wish to thank the german science foundation for support in the frame of project A2 in Sonderforschungsbereich 616 at the University of Essen.

References

[1] V. Agarwal, Thin Solid Films 24 (1974) 55.
[2] P. Solomon, J. Vac. Sci. Technol. 14 (1977) 1122.
[3] N. Klein, in: L. Marton (Ed.), Advances in Electronics and Electron Physics, vol. 26, Academic Press, New York, 1969, p. 133.
[4] T. DiStefano, M. Schatzkes, J. Vac. Sci. Technol. 13 (1976) 50.
[5] S. Ikonopisov, Electrochim. Acta 22 (1977) 1077.
[6] V. Parkhutik, J. Albella, J.M. Duart, in: B. Conway (Ed.), Modern Aspects of Electrochemistry, vol. 23, Plenum Press, New York, 1992, p. 315.
[7] M.A. Alam, R.K. Smith, B.E. Weir, P.J. Silverman, Nature 420 (2002) 378.
[8] P.A. Packan, Science 285 (1999) 2079.
[9] L. Dissado, P. Sweeney, Phys. Rev., B 48 (1993) 16261.
[10] R. Cafiero, A. Gabrielli, M. Marsili, M.A. Muñoz, L. Pietronero, Phys. Rev., B 60 (1999) 786.
[11] M. Hastings, Phys. Rev. Lett. 87 (2001) 175502.
[12] K. McKinley, N. Sandler, Thin Solid Films 290–291 (1996) 440.
[13] P. Rottländer, M. Hehn, O. Lenoble, A. Schuhl, Appl. Phys. Lett. 78 (2001) 3274.
[14] S. Ezhilvalavan, T.-Y. Tseng, Thin Solid Films 360 (1999) 268.
[15] R. Fleming, D. Lang, C. Jones, M. Steigerwald, D. Murphy, G. Alers, Y. Wong, R. van Dover, J. Kwo, A. Sergent, J. Appl. Phys. 88 (2000) 850.
[16] J. Chang, M. Steigerwald, R. Fleming, R. Opila, G. Alers, Appl. Phys. Lett. 74 (1999) 3705.
[17] S. Zafar, E. Cartier, E. Gusev, Appl. Phys. Lett. 80 (2002) 2749.
[18] A.W. Hassel, D. Diesing, Electrochem. Commun. 4 (2002) 1.
[19] D. Diesing, A.W. Hassel, M.M. Lohrengel, Thin Solid Films 342 (1999) 283.
[20] M.M. Lohrengel, Mater. Sci. Eng., R 11 (1993) 243.
[21] A. Hassel, D. Diesing, Thin Solid Films 414 (2002) 296.
[22] D. Diesing, G. Kritzler, M. Stermann, D. Nolting, A. Otto, J. Solid State Electrochem. 7 (2003) 389.
[23] R.H. Fowler, L. Nordheim, Proc. R. Soc. 119 (1928) 173.
[24] J. Schäfer, C. Adkins, J. Phys.: Condens. Matter 3 (1991) 2907.
[25] N. Ashcroft, N. Mermin, Solid State Physics, Holt Saunders International Editions, Philadelphia, 1976, p. 38, Ch. 1.
[26] N. Ashcroft, N. Mermin, Solid State Physics, Holt Saunders International Editions, Philadelphia, 1976, p. 5, Ch. 1.
[27] E. Wolf, Principles of Electron Tunneling Spectroscopy, Oxford University Press, Oxford, 1985, p. 22, Ch. 5.
[28] J. Sakurai, Modern Quantum Mechanics, Addison Wesley, 1994.
[29] F.P. Fehlner, Low Temperature Oxidation: The Role of Vitreous Oxide, Wiley, London, 1986.
[30] A. Jonscher, Universal Relaxation Law, Chelsea Dielectrics Press, London, 1996.
[31] H. Böttger, V.V. Bryskin, Hopping Conduction in Solids, Akademie Verlag, Berlin, 1985.
[32] A. Wehner, Y. Jeliazova, R. Franchy, Surf. Sci. 531 (2003) 287.
[33] J. Simmons, G. Taylor, Phys. Rev., B 5 (1972) 553.